LA-10453-MS

Los Alamos National Laboratory is operated by the University of California for the United States Department of Energy under contract W-7405-ENG-36

The BDD II: An Improved Electron Dosimeter for the Global Positioning System

Los Alamos
Los Alamos National Laboratory
Los Alamos, New Mexico 87545

LA-10453-MS

UC-37
Issued: July 1985

The BDD II: An Improved Electron Dosimeter for the Global Positioning System

W. Feldman
W. Aiello
D. Drake
M. Herrin

Los Alamos National Laboratory
Los Alamos, New Mexico 87545

THE BDD II: AN IMPROVED ELECTRON DOSIMETER FOR THE GLOBAL POSITIONING SYSTEM

by

W. Feldman, W. Aiello, D. Drake, and M. Herrin

ABSTRACT

This report describes the design, operation, and on-line data reduction procedures for BDD II, an electron/ion dosimeter for the Block II version of the Global Positioning System.

I. INTRODUCTION

Energetic electron/ion dosimeters are to be flown aboard 3 of the 18 satellites that constitute the US Air Force Global Positioning System (GPS). The purpose of these dosimeters (BDD) is to continuously monitor the radiation background experienced by all of the GPS satellites. The resultant levels of measured omnidirectional electron fluxes then allow a determination of the integrated radiation dose absorbed by system electronic components. A knowledge of the radiation hardness of the sensitive components that could cause a failure then allows an estimate of the mean time to satellite failure or, in other words, a probable value for the remaining lifetime of each satellite in the system.

The first model of this instrument, the BDD I, is presently operating successfully in orbit. It was designed to meet the objectives just stated. However, it was included as a retrofit to an already designed Block I system. It was therefore subject to several interface constraints that, in turn, dictated limitations in detector performance. Many of these constraints have

since been relaxed in the Block II GPS spacecraft. This has allowed the design of an improved dosimeter, the BDD II, which will provide

- Increased resolution of the fluxes of electrons having energies above ~1.5 MeV. These electrons have the largest potential for damage to electronic components, and they will provide the most sensitive discriminators for the identification of a fission beta-decay electron source.
- A direct measurement of the differential energy spectrum. This will remove ambiguities in data reduction and hence facilitate on-line damage assessment.
- A capability for identifying a fission beta-decay spectrum. Such a spectrum has been observed after past high-altitude nuclear weapons tests.

II. DESIGN REQUIREMENTS

A. Programmatic Objectives

The orbits of Block II GPS satellites are circular with an altitude of 11 000 nautical miles and an inclination of 55°. As such, they pass through the peak intensity region of the Earth's magnetically trapped radiation belt twice per 12-h orbit. This property of the orbits chosen for the GPS satellites provides the primary rationale for including an electron dosimeter as part of their payload complement to provide an on-line radiation damage assessment capability.

Energy spectra of trapped electrons predicted by a few of the current models at this peak of the terrestrial radiation belts are shown in Fig. 1 (Argo et al., 1980). The particle fluxes at the GPS orbit are known to vary with solar activity and with geomagnetic latitude. The spectra shown in Fig. 1 are for equatorial latitudes at an altitude of 11 000 nautical miles during solar maximum in 1967. They were calculated using the AE-4 model of Singley and Vette (1972) and were augmented using a preliminary version of the AE-7 model.* Superimposed on these spectra is the AE-4 10% probability curve. This curve represents the model electron spectrum that will be exceeded 10% of the time. Also included is the proton energy spectrum observed between August 4-9, 1972, during the most intense high-energy proton events ever recorded near the Earth. The endpoints of the seven electron energy levels and four proton energy levels of the BDD II are indicated in Fig. 1 for reference purposes.

*This information was supplied by S. B. Roeske, Sandia National Laboratories, Albuquerque.

Although intense fluxes of energetic heavy ions have been shown to trigger logics upsets in several satellites operating at synchronous orbit (Baker, 1984), energetic electrons are known to be responsible for most of the accumulated, irreversible radiation damage that causes the catastrophic failures in spacecraft electronics. It is also known that susceptibility to such failures per incident electron is an increasing function of electron energy. This fact is shown in Fig. 2 using a dose conversion factor, $\eta(E)$, calculated for an unshielded CMOS component and normalized to 1 at 1 MeV. The accumulated radiation dose giving the net damage suffered by a component directly exposed to radiation in the form of a differential electron flux energy spectrum, such as displayed in Fig. 1, is therefore given by the summed product of the dose conversion factor with the time-integrated differential flux spectrum. This flux spectrum, accumulated over time interval Δt at time t_i, is denoted by $F(E,t_i)\Delta t$. Then the radiation dose, $D(T)$, accumulated over m time intervals by a bare electronic component, is given by

$$D(T) = \int_0^\infty \eta(E)\, J_m(E)\, dE \ , \tag{1}$$

where

$$J_m(E) = \sum_{i=1}^{m} F(E,t_i)\Delta t \tag{2}$$

is the time-integrated flux spectrum or differential energy spectrum of electron fluence and $T = m\Delta t$.

Estimation of the integrated dose experienced by an arbitrary component of a spacecraft is similar to that just described, but it requires one additional step. Since most components will be at least partially shielded from the external radiation environment by spacecraft materials, a faithful estimate requires incorporation of the spacecraft geometry into a combined energetic electron x-ray radiation transport computer code (Hollars et al., 1977). The end result of these calculations is a set of dose conversion factors, $\eta_i(E)$, for each of the i spacecraft positions where the sensitive electronic components are known to be located. Then the radiation dose accumulated at each of these i locations is given by

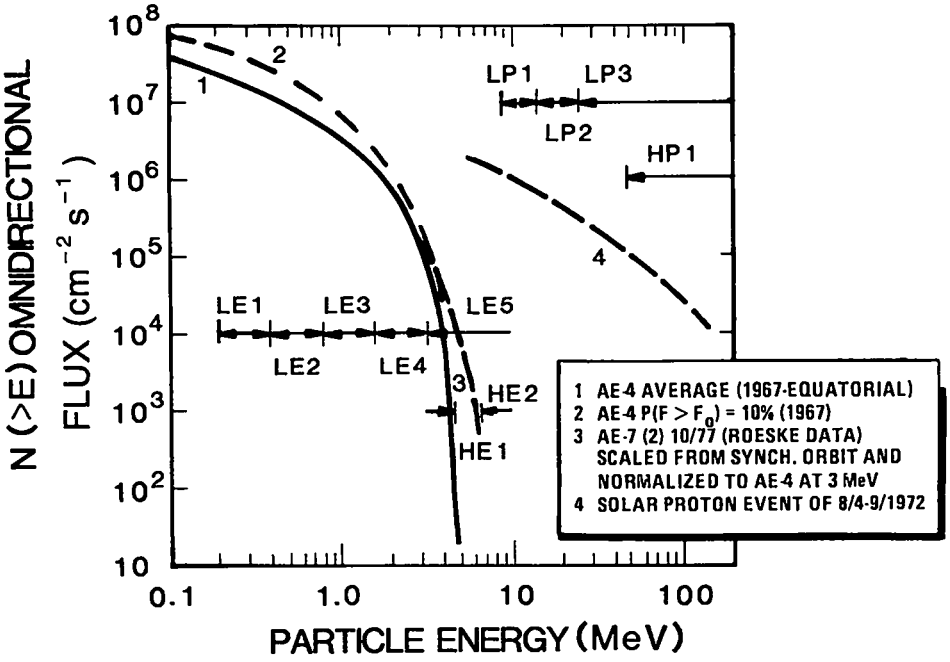

Fig. 1. Energy spectra of trapped electrons along the geomagnetic equator at an altitude of 11 000 nautical miles as predicted by current models. The dashed curve labeled 4 shows a proton spectrum measured during the giant solar proton event of August 4-9, 1972.

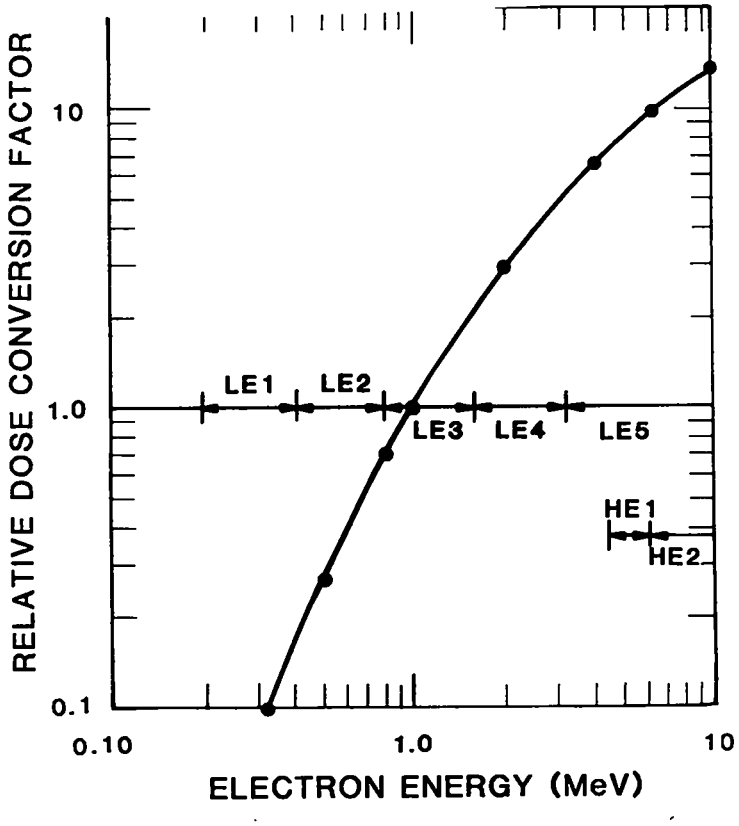

Fig. 2. The dose conversion factor for a CMOS component normalized to 1 at 1 MeV.

$$D_i(T) = \int_0^\infty \eta_i(E)\, J_m(E)\, dE \ . \qquad (3)$$

A secondary goal of the BDD II is to identify fission beta-decay electron spectra. Such spectra result from the high-altitude detonation of a nuclear weapon. Their dependence on energy depends on distance relative to the L-shell of the explosion and the time since detonation. A few representative examples, measured on December 8, 1962, nearly 5 months after the Starfish test that occurred on July 9, 1962, are shown in Fig. 3 (Hess, 1968). Detonation during this test occurred at an altitude of 400 km at L = 1.12. The spectra labeled B, C, and D were measured at L = 1.25, 1.34, and 1.57, respectively. They are compared with the shape of an equilibrium-fission energy spectrum given by the dashed curve labeled A. The following generalizations can be drawn from Fig. 3: (1) electron fluxes decrease with increasing distance (L-shell) from the explosion; (2) the low-energy parts of the spectra are attenuated most at the low L-shells due to Coulomb scattering into the atmospheric loss cone; and (3) the high-energy parts of the beta-decay spectra labeled B and C are

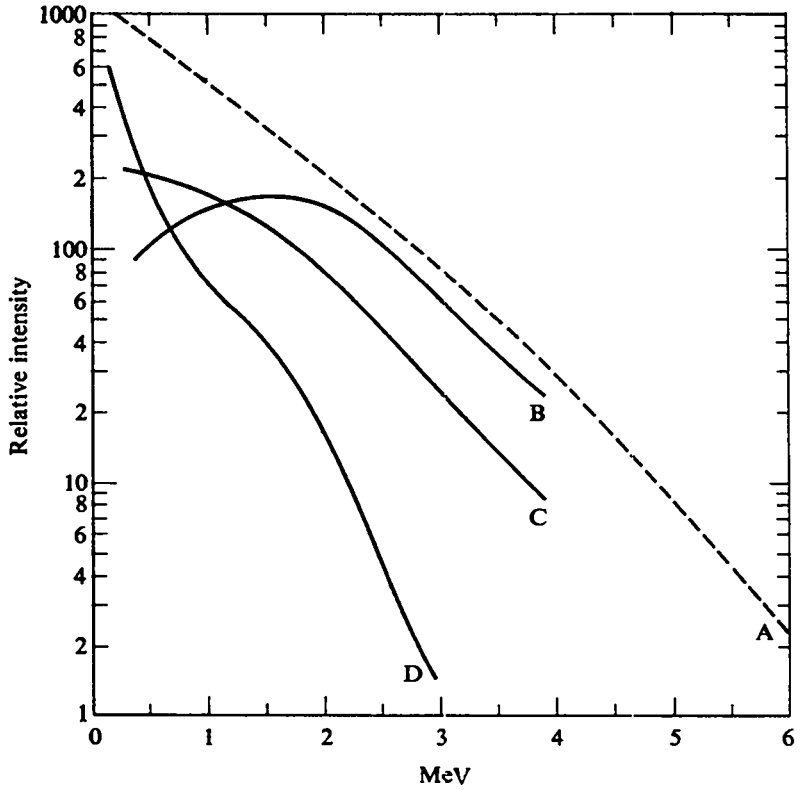

Fig. 3. Fission beta-decay electron spectra measured at several L-shells on December 8, 1962, nearly 5 months after the Starfish high-altitude nuclear test.

considerably enhanced over comparable parts of naturally occurring spectra that are very similar to D.

Measurements of electrons injected into the inner magnetosphere to form artificial radiation belts from a variety of high-altitude nuclear weapons tests have shown that, at the L-shell of GPS, the mean lifetime of ~2 MeV electrons is about 1 month. Thus, if such a belt were formed, it could significantly increase the fluence of energetic electrons encountered by the GPS satellites. Such an event would therefore reduce their lifetimes. In order to model this belt to predict its effect on all the GPS satellites as well as on other important systems, it is important both to identify the spectrum as caused by fission beta decay and to determine its intensity as a function of L-shell.

B. BDD II Measurement Objectives

The foregoing considerations dictated the measurement objectives of BDD II. First priority, therefore, was to determine the differential energy spectrum of energetic electrons. This objective satisfies both the requirement to obtain a differential fluence spectrum for dose estimation and the requirement to identify a fission electron spectrum resulting from a nuclear weapons test. The electron spectra in Fig. 1 combined with the unshielded dose conversion factor in Fig. 2 provide guidelines to cover a useful energy range, $0.3\ \text{MeV} \lesssim E \lesssim 10\ \text{MeV}$. This same range is also optimum for discriminating fission electron spectra from naturally occurring spectra (see, e.g., Fig. 3) since the average energy of fission beta-decay electrons is about 1 MeV.

Second priority for the BDD II was to measure the spectrum of energetic ions. The shape of the spectrum given by curve 4 in Fig. 1, coupled with the fact that protons with energy $\lesssim$10 MeV are not very penetrating and therefore do not pose a serious problem for electronic upsets in spacecraft systems, suggests an ion energy range spanning ~10 MeV to ~100 MeV.

Subsidiary but important design requirements to meet the BDD II measurement objectives include (1) a small enough geometric factor to prevent saturation at conservative estimates of the highest expected electron fluxes, (2) provision for shielding adequate for a $\gtrsim$5-year detector lifetime, (3) use of sensors that are relatively immune to environmental damage, and (4) a requirement for spacecraft resources within the limits allowed by the Block II system design.

III. THE BDD II DESIGN

A. Mechanical Design

The BDD II is a compact, two-element particle spectrometer sensitive to both electrons and ions as shown in Figs. 4 and 5. It consists of two identical scintillator assemblies sensitive to high-energy and low-energy particles, respectively. The two energy ranges are required to provide accurate measurements of electron fluxes over the dynamic range (~8 orders of magnitude) spanned by the spectra in Fig. 1. Each assembly is composed of two nested plastic scintillators encased in Be shields. These shields were designed to provide suitable geometric factors for the ranges of electron fluxes expected along the GPS orbits. Both sensor assemblies will have the same field of view consisting of approximately 60° half-angle cones pointing along the -X-direction of the satellite. A drawing of these assemblies is given in Fig. 4, and their position in the instrument is shown in Fig. 5.

The outer components of each of the nested scintillator pairs is a 30-mil-thick plastic scintillator shell. Its purpose is to provide a signal sufficient to separately identify electrons from ions. This purpose is readily achieved because ions within the energy range detected by the BDD II instrument deposit much more energy upon passage through the shell than do electrons. For example, given an event in the inner scintillator having a light output equivalent to an ~800-keV electron, a proton would have resulted in a signal in the shell more than 35 times greater than that which would have been produced by an electron.

The inner component of each of the nested pairs is a solid plastic scintillator having a minimum path length (at 0° incidence) of 1.55 g/cm^2. This length corresponds to the range of a 3.1-MeV electron. For all incident electrons having energy sufficient to penetrate the shell and deposit a sensible amount of energy in the inner scintillator, the energy lost in the shell is roughly constant at about 150 keV. In consequence, the pulse height of the inner scintillator yields a faithful representation of the total energy of the incident electrons up to ~3.25 MeV. This property of the detector assembly is used to define the energies of incident electrons. However, this property does not hold for ions. In this case, though, the energy deposited in the shell scintillator is a monotonically decreasing function of increasing ion energy. Thus, the pulse height in the inner scintillator yields a unique measure of the total energy of incident ions. It therefore can be used to

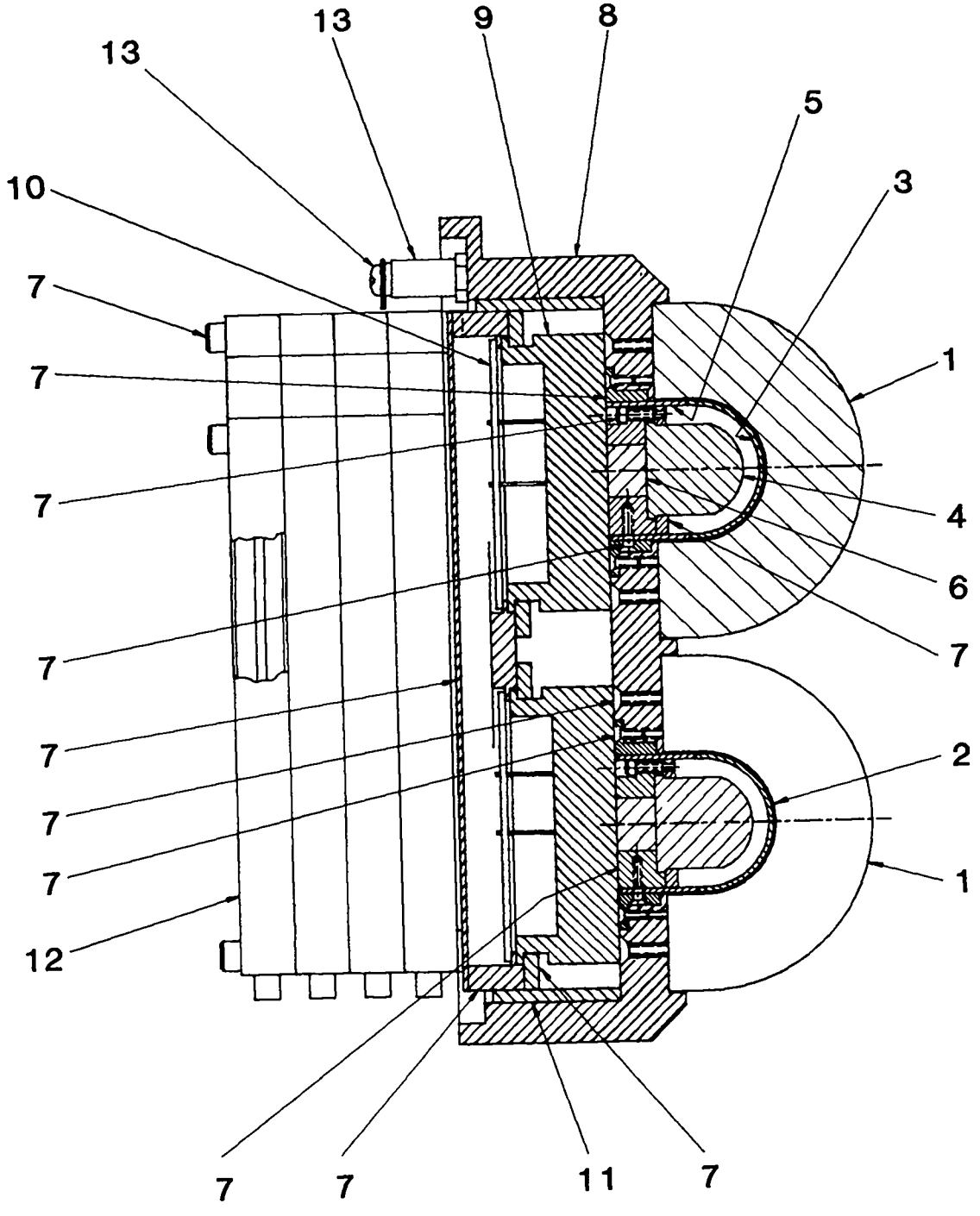

Fig. 4. Details of the two sensor assemblies of BDD II showing (1) the Be radiation shield, (2) the Kel F-light shield, (3) the shell scintillator, (4) the central scintillator, (5) the Lucite shell light guide, (6) the cylindrical Lucite light guide for the central scintillator, (7) scintillator assembly retainer hardware, (8) an Al shield for the microchannelplate photomultiplier tubes (MCPPMTs), (9) the MCPPMTs, (10) MCPPMT bleeder board, (11) a Kel F-insulator, (12) the front-end preamplifiers and amplifiers for the electronics, and (13) the high-voltage terminal.

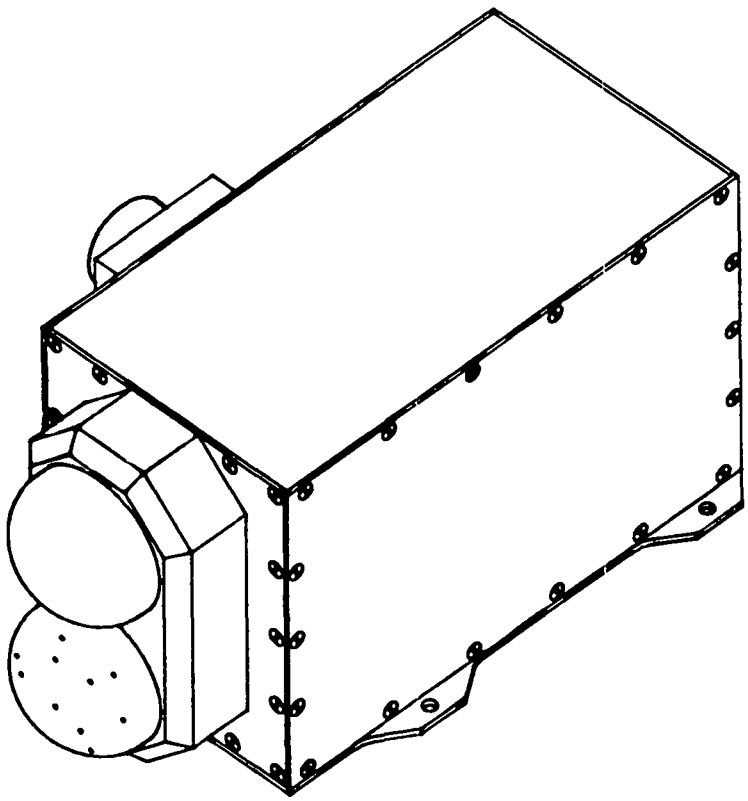

Fig. 5. An outside view of the BDD II showing the 15 holes in the low-energy sensor (bottom left) that are fitted with Au-insert cylindrical collimators.

define ion energies up to a maximum set by the minimum thickness of the detector, ~50 MeV.

Each of the nested pairs of scintillators is viewed by a microchannel plate photomultiplier tube (MCPPMT). The particular tubes used in the BDD II are fitted with split anodes consisting of a center circle nested within a concentric annulus. The Lucite elements of the sensor assemblies, which couple the light from the scintillators to the MCPPMT, are designed to provide output pulse heights that faithfully represent the energy input to the inner and outer scintillators. Laboratory measurements have shown that the crosstalk between signal channels is about 5% and is therefore not a problem in this application.

The Be shields surrounding each scintillator assembly have identical dimensions. Their only difference is that one is solid (the high-energy assembly) and the other has 15 holes (the low-energy assembly). These holes are threaded with hollow Au inserts to define a total area/solid angle acceptance which is reduced from that of the bare assembly by close to four orders of magnitude. Their placement is such as to represent equal solid angles within a 60° half-angle acceptance cone.

Because of the holes in the Be shield of the low-energy assembly, the minimum detectable energy is determined by that required to penetrate a 10-mil-thick Kel F-light shield surrounding the outer shell and then to provide a pulse large enough to trigger a low-level discriminator in the electronics. This energy is approximately 250 keV for electrons and approximately 4.5 MeV for protons. On the other hand, all particles have to penetrate a 1.5-cm-thick Be shield in addition to the Kel F-shield before entering the scintillator shell in the high-energy assembly. The minimum detectable energies in this assembly are therefore about 4.5 MeV for incident electrons and about 55 MeV for incident protons.

High-energy electrons have access to the whole scintillator assembly in the high-energy sensor although they have to penetrate the Be shield. The solid angle/total area geometric factor for these electrons is therefore close to 10^4 times larger than that for the low-energy electrons in the low-energy sensor. This factor of 10^4 nearly compensates for the lower flux levels of the high-energy electrons in the terrestrial radiation belts as seen in Fig. 1. The total counting rates in both sensors should therefore be comparable. However, high-energy electrons should also penetrate the solid portions of the low-energy Be shield. This penetration then contributes a significant background to the low-energy electron count rates in the low-energy sensor. Because the high-energy sensor is designed to be both physically and electronically identical to the low-energy sensor, this background will be measured and subsequently subtracted from the low-energy count rates in the data analysis. The background-subtracted low-energy count rates then yield accurate determinations of the differential electron energy flux spectrum from about 0.25 MeV to about 4 MeV.

B. Electronics Design

A block diagram of the electronics is shown in Fig. 6. The analog signals from the annulus-shaped anode (coupled to the shell scintillator) and the central anode (coupled to the central solid scintillator) are fed into a bank of energy-level discriminators by means of their associated preamplifier and amplifier chains. The digital output of these discriminators allows first an identification of each event as caused by either an electron or an ion and then a sorting in accordance with the energy that they deposit in the solid scintillator. Each event is stored in counting registers in accordance with

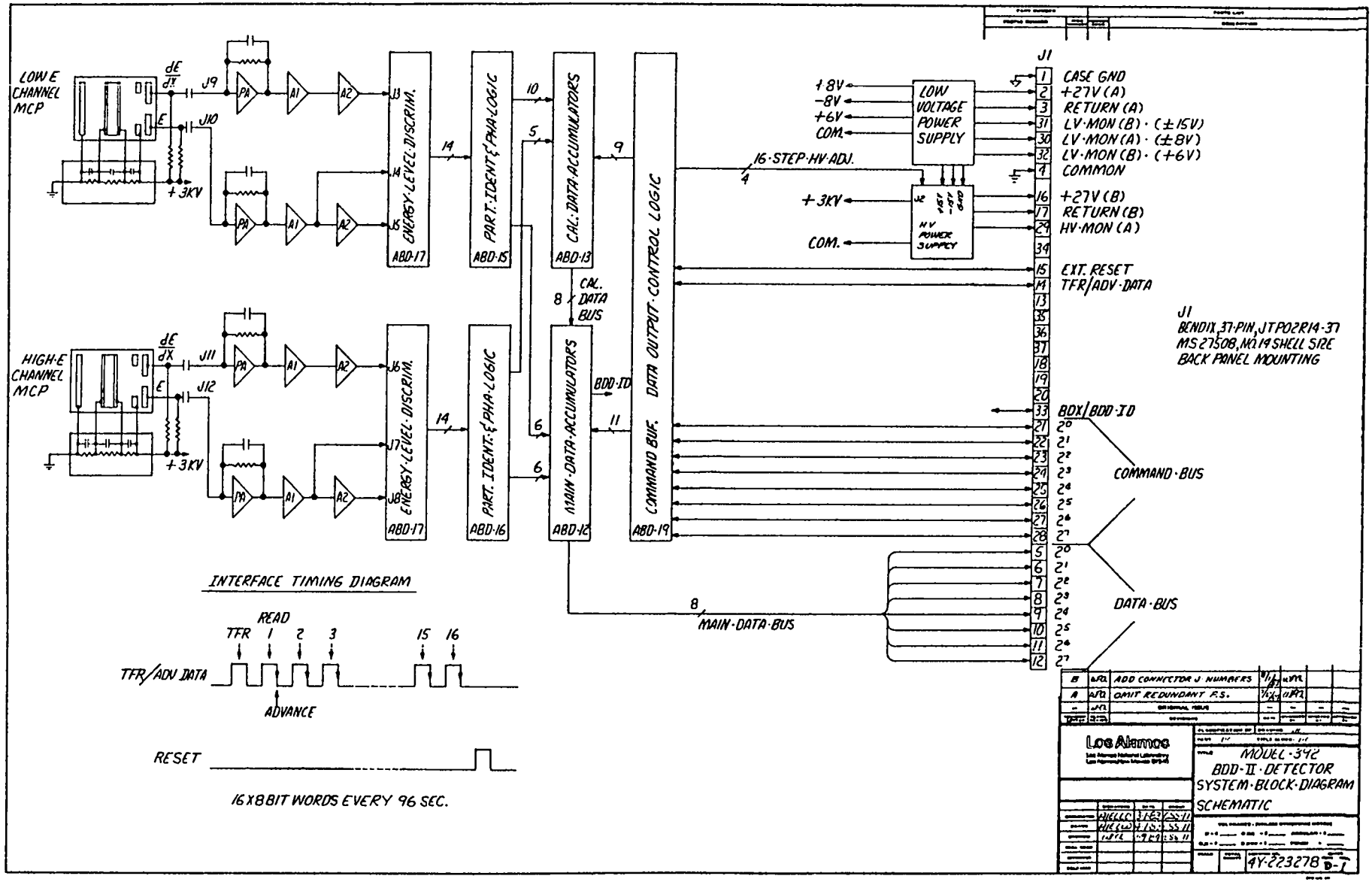

Fig. 6. Block diagram of the BDD II electronics.

its particle type and energy identification. The number of pulses accumulated in each of these registers during the accumulation interval (96 s) provides the data in this experiment from which the electron and ion spectra are obtained.

Energy calibration will be maintained by monitoring the annulus pulse heights. These amplitudes should peak at a level corresponding to about 150 keV, the energy deposited by most electrons in the shell scintillator. If this peak height should change, the high-voltage bias on the MCPPMTs will be adjusted by ground command. Sixteen steps from 2400 V to 3000 V, corresponding to 40 V per step, were designed into the bias supply for this purpose. The corresponding command list recognized by the BDD II logics is given in Table I.

C. Data Output

Data words from the BDD II are organized into major data frames that repeat every 16 × 96 = 1536 s (25.6 min). Each major data frame consists of 16 × (16-8 bit bytes) as shown in Fig. 7. Thirteen of the 16-byte words repeat identically every 96 s. Their physical identification is given in words 1 through 11 in Table II. The lowest-energy words for both the low-energy and high-energy sensors, LE1 and HE1, respectively, use the full 16-bit capability of the Utopia scaler developed recently by P. Beck of Sandia National Laboratories, Albuquerque. The low-order (L) and high-order (H) parts of these words appear in locations 1, 2 and 9, 10 respectively. Singles data from the central (S1) and shell (S2) scintillators are interleaved in words 11 and 12 of alternate 16-byte sequences. Calibrate words C1 through C12 along with 4 sync tags are subcommutated in the 16th word of each of the 16-byte sequences. Their definitions are collected in Table III.

Input counts are compressed by the Utopia scaler using the square root function. The correspondence between input, x, and output, z, counts is given by z = integer value of $\sqrt{x}$ with the exception that z = 1 when x = 0.

TABLE I

8-BIT COMMAND LIST

Binary	HEX	Function
$(0000\ 0000)_2$	$(00)_{16}$	hv set to 2400 V
$(0000\ 0001)_2$	$(01)_{16}$	hv set to 2440 V
.	.	.
.	.	.
.	.	.
.	.	.
$(0000\ 1110)_2$	$(0E)_{16}$	hv set to 2960 V
$(0000\ 1111)_2$	$(0F)_{16}$	hv set to 3000 V

TABLE II

MAJOR FRAME WORD IDENTIFICATIONS

Word	Symbol	Particle Type	Energy Range (MeV)
1	LE1	Electron	0.2 - 0.4
2	LE2	Electron	0.4 - 0.8
3	LE3	Electron	0.8 - 1.6
4	LE4	Electron	1.6 - 3.2
5	LE5	Electron	>3.2
6	LP1	Proton	9 - 15
7	LP2	Proton	15 - 25
8	LP3	Proton	>25
9	HE1	Electron	4.5 - 5.9
10	HE2	Electron	>5.9
11	HP1	Proton	>50
12	LES1	Singles	---
13	LES2	Singles	---
14	HES1	Singles	---
15	HES2	Singles	---

WORD	1	2	3	4	5	6	7	8	9	10	11	12	13	14	15	16	WORD
1	LE1 (L)	HE1 (L)	LE2	LE3	LE4	LP1	LP2	LP3	LE1 (H)	HE1 (H)	LE S1	HE S1	LE5	HE2	HP1	CAL TAG	16
17	LE1 (L)	HE1 (L)	LE2	LE3	LE4	LP1	LP2	LP3	LE1 (H)	HE1 (H)	LE S2	HE S2	LE5	HE2	HP1	CAL TAG	32
33											LE S1	HE S1				C1	48
49											LE S2	HE S2				C2	64
65											LE S1	HE S1				C3	80
81											LE S2	HE S2				C4	96
97											LE S1	HE S1				C5	112
113											LE S2	HE S2				C6	128
129											LE S1	HE S1				C7	144
145											LE S2	HE S2				C8	160
161											LE S1	HE S1				C9	176
177											LE S2	HE S2				C10	192
193											LE S1	HE S1				C11	208
209											LE S2	HE S2				C12	224
225	LE1 (L)	HE1 (L)	LE2	LE3	LE4	LP1	LP2	LP3	LE1 (H)	HE1 (H)	LE S1	HE S1	LE5	HE2	HP1	CAL TAG	240
241	LE1 (L)	HE1 (L)	LE2	LE3	LE4	LP1	LP2	LP3	LE1 (H)	HE1 (H)	LE S2	HE S2	LE5	HE2	HP1	CAL TAG	256

Fig. 7. Detailed format of the BDD II data frame.

TABLE III

DEFINITION OF CALIBRATE WORDS

Symbol	Sensor	Particle Type	DE Level	E Level
C1	LE	Electron	(1 to 2)	(1 to 5)
C2	LE	Electron	(2 to 3)	(1 to 5)
C3	LE	Both	(3 to 4)	(1 to 5)
C4	LE	Electron	(1 to 3)	(5 to 6)
C5	LE	Proton	>3	(5 to 6)
C6	LE	Electron	(2 to 3)	(5 to 6)
C7	HE	Electron	(1 to 2)	(1 to 5)
C8	HE	Electron	(2 to 3)	(1 to 5)
C9	HE	Both	(3 to 4)	(1 to 5)
C10	HE	Electron	(1 to 3)	(5 to 6)
C11	HE	Both	>3	(5 to 6)
C12	HE	Electron	(2 to 3)	(5 to 6)

IV. DATA ANALYSIS

The purpose of the BDD II on-line reduction algorithm is to provide both an electron differential fluence energy spectrum, $J_m(E)$, and a running radiation-dose index, D_m, to help estimate the useful life remaining for the various spacecraft of the GPS. As explained in Section II, $J_m(E)$ is related to the measured instantaneous differential energy flux spectra $F(E,t_i)$ through Eq. (2), and D_m is related to J_m and the appropriate dose conversion factor, $\eta(E)$, through Eq. (1). These relations are approximated by the following digitized forms in the on-line data reduction algorithm for the BDD II dosimeter:

$$D(T) = \sum_{j=1}^{7} \eta_j J_{mj}(T) \Delta E_j \ ; \tag{4}$$

$$J_{mj}(T)\Delta E_j = \sum_{i=1}^{m} F_j(t_i)\Delta t \ \Delta E_j \ ; \text{ and} \tag{5}$$

$$F_j(t_i)\Delta E_j = (C_j - B_j)/G_j \ . \tag{6}$$

Here, the total time since launch is $T = m\Delta t$, where $\Delta t = 96$ s, the smallest BDD II integration time. The η_j is a tabular array stored in a data statement giving the energy-dependent dose conversion factors evaluated at the midpoints of each of the BDD II electron energy intervals, $1 \leq j \leq 7$. The G_j, $1 \leq j \leq 7$, is another stored data array giving the instrumental energy-dependent geometric factors. The C_j, $1 \leq j \leq 7$, are the counts accumulated in 96 s in each of the energy-sorted electron-counting registers. The B_j, $1 \leq j \leq 7$, is a background for the low-energy sensor representing energetic electrons penetrating the solid portion of the low-energy Be shield. Because only high-energy electrons are counted by the high-energy sensor, $B_6 = B_7 = 0$. The background for the low-energy sensor is estimated as follows. We assume for background estimation purposes only that the flux at high energies has the form

$$F(E,t_i) = AE^{-(\alpha+1)} \quad . \tag{7}$$

Then the counts registered in the two energy channels of the high-energy sensor, $j = 6,7$, can be approximated by

$$C_j \simeq G_j \int_{E_j}^{E_{j+1}} F(E,t_i)dE \quad . \tag{8}$$

Inserting Eq. (7) into Eq. (8) and noting that $E_8 = \infty$ and that $G_6 = G_7 = G_H$, we get

$$C_7 = \frac{G_H A}{\alpha} E_7^{-\alpha} \tag{9}$$

and

$$C_6 + C_7 = \frac{G_H A}{\alpha} E_6^{-\alpha} \quad . \tag{10}$$

Then

$$\alpha = \frac{\ell n[1 + C_6/C_7]}{\ell n(E_7/E_6)} \tag{11}$$

and

$$\frac{G_H A}{\alpha} = (C_6 + C_7)\, E_6^{+\alpha} \, . \tag{12}$$

Since the high-energy and low-energy sensors are physically identical, the high-energy electrons, which cause a background in the low-energy sensor, have energies $E_{Bj} = E_j + \delta E_j$, where the δE_j is a tabular array whose elements are all approximately equal to 4.3 MeV. This value corresponds to the minimum energy electron that can penetrate the solid portion of the low-energy Be shield. The low-energy background can therefore be approximated by

$$B_j = G_H \frac{A}{\alpha} \left[E_{Bj}^{-\alpha} - E_{Bj+1}^{-\alpha}\right] \, . \tag{13}$$

Substituting Eq. (12) into Eq. (13) yields

$$B_j = (C_6 + C_7) \left[\left(\frac{E_6}{E_{Bj}}\right)^{\alpha} - \left(\frac{E_6}{E_{Bj+1}}\right)^{\alpha}\right] \, , \tag{14}$$

and α is estimated using Eq. (11). We expect this approximation will not cause unreasonable errors because C_7 appears in a ℓn term in Eq. (11) and then $(C_6 + C_7) \cong C_6$ appears in Eq. (14).

ACKNOWLEDGMENTS

We wish to thank H. Argo, J. Conner, and W. Workman for their support in the development and implementation of this project.

REFERENCES

Argo, H. V., D. N. Baker, R. D. Belian, L. K. Cope, and P. R. Higbie, "The BDD: A Dosimeter for the Global Positioning System," Los Alamos Scientific Laboratory report LA-8421-MS (1980).

Baker, D. N., "Effects of the Solar-Terrestrial Environment on Satellite Operations," in Proceedings of Solar-Terrestrial Prediction Workshop, Meudon, France, 1984. Also Los Alamos National Laboratory document LA-UR-84-3325 (1984).

Hess, W. N., The Radiation Belt and Magnetosphere (Blaisdell Publ. Co., Waltham, Massachusetts, 1968), Chapter 5.

Hollars, D. R., J. R. Janni, and M. F. Schneider, "Degradation of Satellite Electronics Produced by Energetic Electrons," J. Spacecr. Rockets 14, 621, 1977.

Singley, G. W., and J. I. Vette, "The AE-4 Model of the Outer Radiation Zone Electron Environment," National Space Science Data Center report NSSDC 72-06 (1972).

☆ U.S. GOVERNMENT PRINTING OFFICE 1985—576-034/20110

Printed in the United States of America
Available from
National Technical Information Service
US Department of Commerce
5285 Port Royal Road
Springfield, VA 22161

Microfiche (A01)

Page Range	NTIS Price Code	Page Range	NTIS Price Code	Page Range	NTIS Price Code	Page Range	NTIS Price Code
001-025	A02	151-175	A08	301-325	A14	451-475	A20
026-050	A03	176-200	A09	326-350	A15	476-500	A21
051-075	A04	201-225	A10	351-375	A16	501-525	A22
076-100	A05	226-250	A11	376-400	A17	526-550	A23
101-125	A06	251-275	A12	401-425	A18	551-575	A24
126-150	A07	276-300	A13	426-450	A19	576-600	A25
						601-up	A99

Contact NTIS for a price quote.

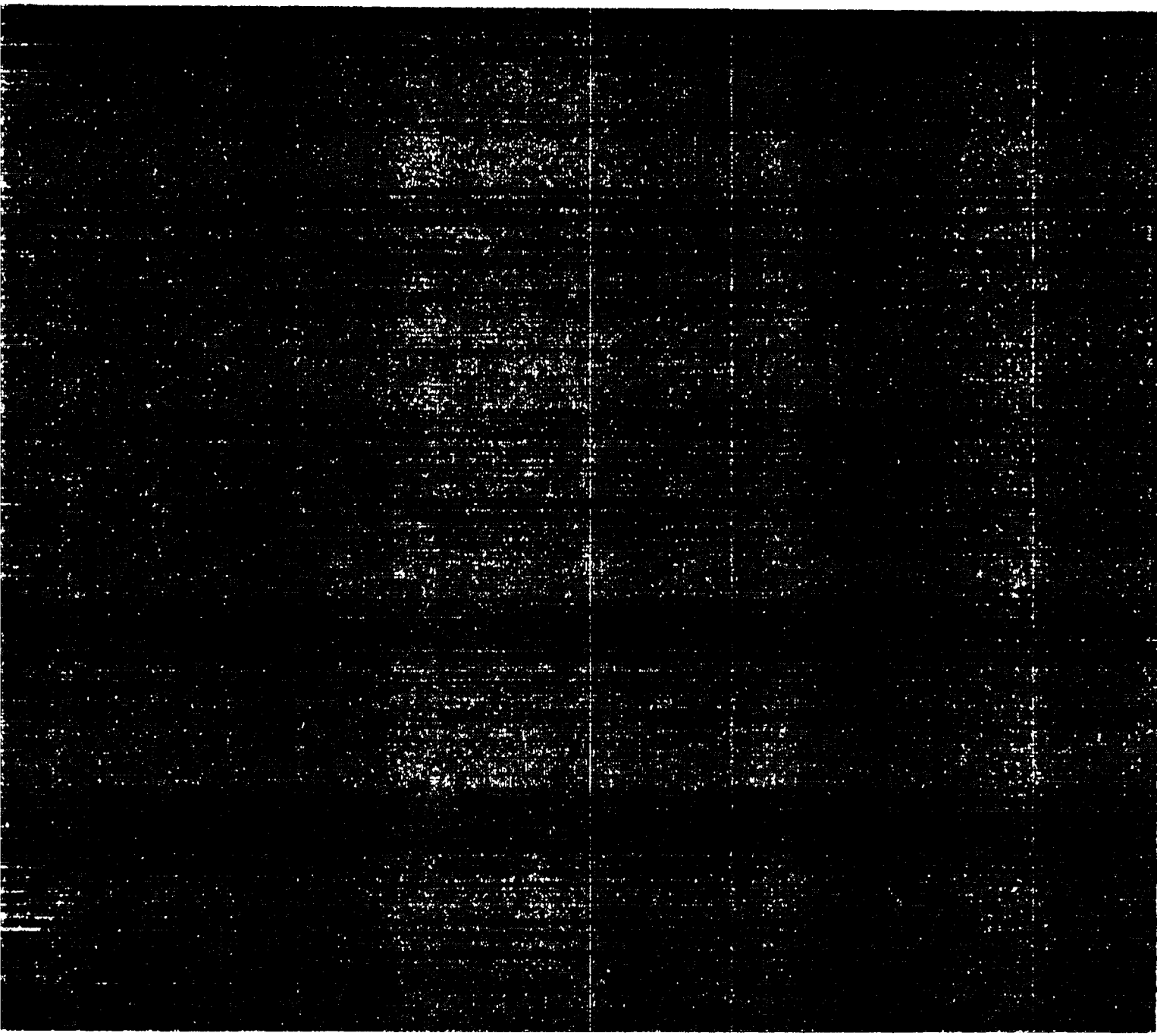

Los Alamos